A novel pattern transfer technique for mounting glassy carbon microelectrodes on polymeric flexible substrates

2016 J. Micromech. Microeng. 26 025018

(http://iopscience.iop.org/0960-1317/26/2/025018)

IOP Publishing Journal of Micromechanics and Microengineering

J. Micromech. Microeng. **26** (2016) 025018 (10pp) doi:10.1088/0960-1317/26/2/025018

A novel pattern transfer technique for mounting glassy carbon microelectrodes on polymeric flexible substrates

Maria Vomero, Pieter van Niekerk, Vivian Nguyen, Nick Gong, Mieko Hirabayashi, Alessio Cinopri, Kyle Logan, Ali Moghadasi, Priya Varma and Sam Kassegne

MEMS Research Lab, Mechanical Engineering Department, College of Engineering, San Diego State University, 5500 Campanile Drive, San Diego, CA 92182-1323, USA

E-mail: kassegne@mail.sdsu.edu

Received 15 September 2015, revised 24 November 2015
Accepted for publication 25 November 2015
Published 12 January 2016

Abstract

We present a novel technology for transferring glassy carbon microstructures, originally fabricated on a silicon wafer through a high-temperature process, to a polymeric flexible substrate such as polyimide. This new transfer technique addresses a major barrier in Carbon-MEMS technology whose widespread use so has been hampered by the high-temperature pyrolysis process (⩾900 °C), which limits selection of substrates. In the new approach presented, patterning and pyrolysis of polymer precursor on silicon substrate is carried out first, followed by coating with a polymer layer that forms a hydrogen bond with glassy carbon and then releasing the ensuing glassy carbon structure; hence, transferring it to a flexible substrate. This enables the fabrication of a unique set of glassy carbon microstructures critical in applications that demand substrates that conform to the shape of the stimulated/actuated or sensed surface. Our findings based on Fourier transform infared spectroscopy on the complete electrode set demonstrate—for the first time—that carbonyl groups on polyimide substrate form a strong hydrogen bond with hydroxyl groups on glassy carbon resulting in carboxylic acid dimers (peaks at 2660 and 2585 cm^{-1}). This strong bond is further confirmed by a tensile test that demonstrated an almost perfect bond between these materials that behave as an ideal composite material. Further, mechanical characterization shows that ultimate strain for such a structure is as high as 15% with yield stress of ~20 MPa. We propose that this novel technology not only offers a compelling case for the widespread use of carbon-MEMS, but also helps move the field in new and exciting directions.

Keywords: MEMS, C-MEMS, polyimide, neural probe, glassy carbon, SU-8, pyrolysis

(Some figures may appear in colour only in the online journal)

1. Introduction

The field of carbon-MEMS (C-MEMS), which involves the patterning of a photosensitive polymer precursor on a silicon substrate followed by pyrolysis of the polymer layer to convert it to glassy carbon, has not only gained traction but is also seeing an increased range of applications varying from fuel cells [1, 2], organic solar cells [3], and electrodes for dielectrophoretic cell separation systems [4, 5], to bio-nano-electronics platforms [6, 7] and neural electrodes [8, 9].

However, one of the inherent challenges in this fabrication process is the high-temperature (⩾900 °C) required for pyrolysis during conversion of a polymer cursor to glassy carbon [10, 11]. As a result, this has constrained C-MEMS microstructures to be fabricated and mounted typically on rigid substrates such as silicon and quartz which have a

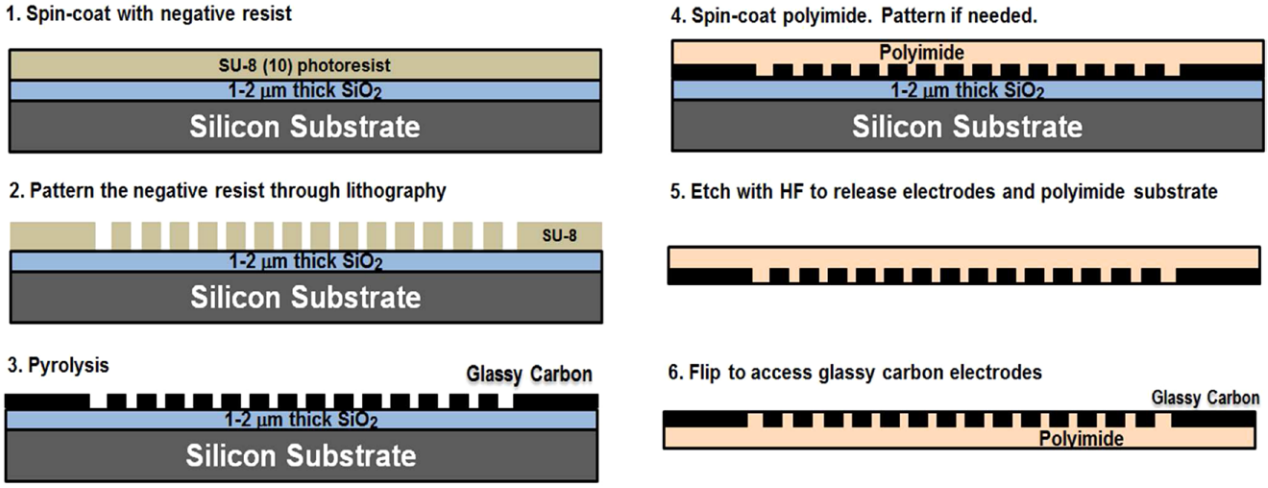

Figure 1. Lithography and pyrolysis process for fabricating glassy carbon electrodes from a negative tone photoresist. Silicon substrate with oxide layer is used. HF etches SiO_2 to release the final structure. The thickness of polyimide substrate is about 20 μm. Polyimide is cured at 375 °C for 2 h in N_2 atmosphere.

high melting point temperature. Therefore, the integration of C-MEMS with (i) variety of flexible or rigid substrates and (ii) a wide range of low-temperature processes such as in CMOS has been unrealized so far. We believe further significant progress in C-MEMS technology can be achieved by finding newer ways to decouple the core high-temperature pyrolysis process from subsequent processes. This could be achieved by first fabricating the glassy carbon structure on a silicon substrate and then transferring the pyrolyzed microstructures to a separate substrate where low-temperature processes could subsequently be carried out. Here, we introduce one such approach where the pattern is transferred to a flexible polymeric substrate such as polyimide. We use polyimide to demonstrate this technology because of its excellent chemical and mechanical durability and patternability through lithography [12, 13]. In a specific research area of interest where glassy carbon electrodes have a superior performance, such as neural probes, this new method could enable fabrication of a complete electrode system with electrodes, traces, and bump pads. This technology is demonstrated here through the microfabrication of a novel glassy carbon-based array of microelectrodes on a polyimide flexible substrate for applications in neural sensing and simulations, particularly for micro-electrocorticography (μECoG) systems [8, 9]. To the best of our knowledge, this is the first reported work in the literature dealing with not only pattern transferring in C-MEMS to flexible substrates, but also the subsequent characterization of the chemical and mechanical bond at the glassy carbon/polyimide interface in the resulting hybrid glassy carbon and polyimide structure.

2. Materials and methods

In this section, we report on the microfabrication steps and the subsequent pattern transfer of glassy carbon microstructures. For demonstrating the technology through an application area of growing research interest, we will use, in the rest of the paper, an example of a series of μECoG microelectrode arrays designed for neural signal recording and stimulation.

Briefly, the microfabrication process is summarized in figure 1. It starts with deposition of SU-8 negative tone resist (20 μm) on a silicon substrate (with 1–2 μm thick oxide) followed by lithography for patterning the microelectrode array. Subsequent to lithography, pyrolysis is carried out in a closed ceramic tube-furnace (Lindberg Division of SBI, Watertown, WI) in vacuum or a forming gas (95% N_2 and 5% H_2) atmosphere through gradual heating to 1000 °C followed by cooling to room temperature [10, 11]. Key parameters such as rate of heating, pressure level, amount of nitrogen flow, and type of substrate are optimized in the pyrolysis process to achieve microelectrodes with excellent conductivity and a strong bond between the substrate and the glassy carbon [8, 9]. The best results are found when SU-8 was heated under continuous nitrogen flow of at least 50 ml min^{-1}. The heating protocol used is: room temperature–700 °C (90 min), 700 °C –900 °C (90 min), 900 °C –1000 °C (90 min), 1000 °C (90 min), 1000 °C –900 °C (90 min), 900 °C –700 °C (60 min), and 700 °C ramped down to room temperature. The pyrolysis process is followed by spin-coating a layer of 20 μm thick photosensitive polyimide (FUJIFilm, Mesa, AZ), degassing and patterning it. If needed, the pattern could contain vias for access for metal traces which can subsequently be patterned through lift-off process. The additional steps in extending this pattern transfer method to layers containing metal traces and bump pads and other additional layers is discussed in separate publications [8, 9]. The polyimide is then cured at 350 °C under nitrogen for 2 h. The devices are released using buffered aqueous HF solution and then soaked in deionized water, cleaned and dried. Polyimide shrinks vertically by about 40%–50% during the curing process, leaving the final polyimide structures less than 10 μm thick [14].

Figure 2 shows the cross-section of the released glassy carbon electrode probe structure. Further details on SEM images of the electrodes after pyrolysis and pattern transfer are also shown in the same figure. In this study, we focus on

Figure 2. (a) Cross-section of pattern transfer process. (b) Shape of the pyrolyzed electrodes is trapezoidal in elevation (conical in 3D) due to uneven shrinking during high-temperature pyrolysis process where both height and diameter decrease significantly. The bottom side that is constrained through attachment to silicon substrate shrinks less as compared to unconstrained sides. (c) Electrodes flush with the polyimide layer.

Table 1. Geometry and process details for probes, S1, S2, and S3 used in characterization experiments.

	Electrode geometry			Process	
Probe type	Diameter (μm)	Spacing (μm)	Width (mm)	Annealing temp. (°C)	Inert environment
S1	300	700	3	275	N_2
S2	150	850	10	350	N_2
S3	180	750	2.5	350	N_2

demonstrating the pattern transfer technique and subsequent characterization through fabrication of three separate neural probes structures with designation of S1, S2, and S3, where each probe differs in geometry and annealing process (table 1). Probe S1 has 300 μm diameter (3 $\times$ 4) electrodes and a width of 3 mm. S2 has 150 μm diameter (32#) electrodes and a width of 10 mm while S3 has (4 $\times$ 4) electrodes with a diameter of 180 μm and width of 2.5 mm. All three probes have breathing holes of 500 μm diameter which allow vascular growth in *in vivo* applications. Figure 3 shows such an electrode-set fabricated using the pattern transfer method described here (S1).

3. Interfacial chemical bond, mechanical, and electrical characterizations

In this section, we investigate and report on the chemical (interface bond), mechanical (modulus, hardness, and tensile strength) and electrical (impedance) characteristics of glassy carbon electrode structures mounted on flexible polyimide substrate.

3.1. Characterization of interfaces between polymer and glassy carbon electrodes

As a background for the chemical bond characterization, we review the chemistry of polyimides. Polyimides are a class of thermally stable and chemically inert polymers that are often based on stiff aromatic backbones consisting of a number of double bonds with flat rings of atoms that form imide functional group –R1–O = CNC = O–R2. Figure 4 is an example of a type of polyimide from DuPont®. The key properties of polyimide are thermoxidative stability, high mechanical strength, high modulus, excellent insulating properties, and superior chemical resistance [15, 16]. The presence of n–π conjugation between non-pair electrons of the nitrogen atom and π electrons of the carbonyl group makes them resistant to chemical agents and moisture [15]. Polyimide, especially the BPDA/PPD type (DuPont's PI2611) has been demonstrated to have biocompatibility, low cytotoxicity and low hemolytic capacity, both for bulk materials and long-term implanted electrodes interfacing with the peripheral and central nervous system [12–17].

The success of the pattern transfer technique presented here strongly depends on the chemical bond between polyimide and glassy carbon, particularly for applications that involve long-term exposure to severe humidity, high-temperature, and chemically-active environments. The literature on the interface between polyimide and glassy carbon, and hence the adhesion characteristics at the interface, is almost non-existent even though there is a substantial amount of work on polyimide and metal interfaces [18–21]. Therefore, this section will focus on determining the chemical basis for the interface between glassy carbon and polyimide. In principle, it is evident that imide group's carbonyl allows (i) dimerization with itself or with another metal or polymer material, and (ii) the forming of a hydrogen bond with hydroxyl groups. Furthermore, weak points in the structure can be broken and form oxygen containing unctuous groups using oxygen plasma. These functional groups along with those that may be present in partially polymerized species also generate opportunities for carbonyl dimerization or hydrogen bonding [22].

The interface characterization will predominantly consist of SEM and FTIR (Fourier transform infrared spectroscopy). SEM will be used to visually establish the attachment of polyimide to glassy carbon in electrode sets where the polyimide is exposed through mechanical tearing. FTIR-ATR (Fourier transform infrared spectroscopy–attenuated total reflectance) will be performed on solid samples through a diamond ATR crystal to determine the nature of chemical bonds that potentially exist between glassy carbon and polyimide.

3.2. Mechanical characterization

The mechanical characterization of the hybrid microstructure consists of determining the Young's modulus and tensile strength through a nanoindentation system and Instron universal testing machine, respectively. All three probe types, i.e. S1, S2, and S3, are tested to determine the effects of geometry and annealing processes on the overall mechanical response of the electrode sets.

3.2.1. Modulus test. The mechanical property, specifically the modulus, is measured using a nanoindentation system that

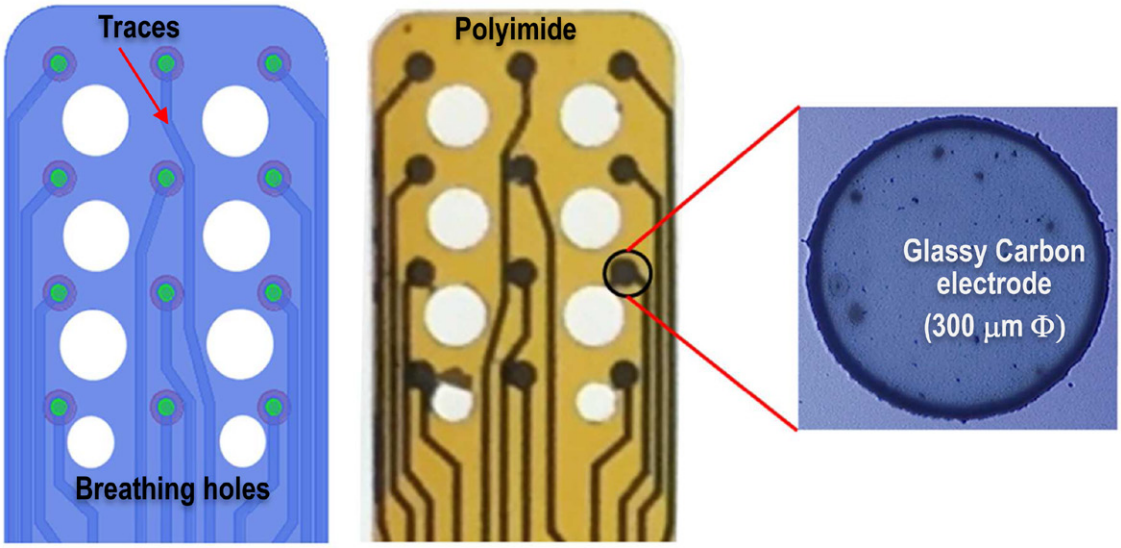

Figure 3. Complete glassy carbon electrode-set fabricated using the pattern transfer method described here. These microelectrode sets shown here (S1) are used for mechanical and electrical characterizations. The traces could be made from glassy carbon or metal [9]. The electrodes have a diameter of 300 μm whereas the traces are 90 μm wide.

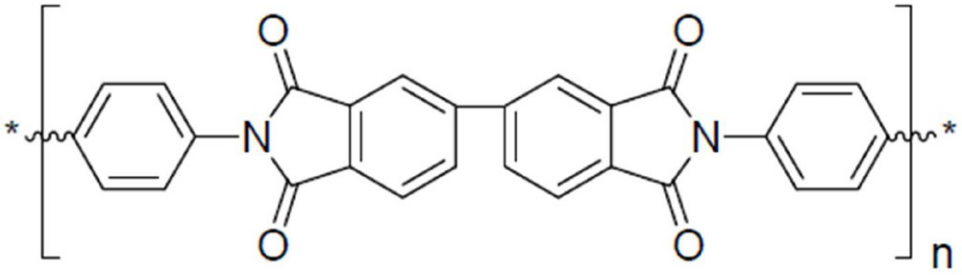

Figure 4. Chemical structure of polyimide BPDA-PPD showing a number of double bonds with flat rings of atoms (DuPont®).

consists of (i) flexure based *XY*-stage for positioning specimen and (ii) flexure-based linear motion stage (*Z*-axis stage) that provides vertical positioning of the tool tip in addition to measuring the contact load of the tool [8, 9]. Load is applied until the indenter stops moving for at least 5 s. A calibrated microscope is used to measure the diamond-shaped indentation marks that correspond to deflection. The modulus is then calculated from the load–deflection relationship. Using this set-up, S3 probes are tested for the modulus.

3.2.2. Tensile test. The Instron 5982 Universal Testing System is used to measure the tensile strength of a series of electrode sets. This model is equipped with a 100 kN load cell and is capable of tensile, compressive, and shears tests at extremely low strain rates. Since the focus of our investigation is to determine the failure modes and the mechanical robustness of a complete microelectrode structure, the specimens used are actual devices with their design dimensions. The testing device itself is composed of a stiff frame with two supports that house the opposite facing jaws of the device. The bottom jaw is static and mounts directly to the frame whereas the upper jaw is affixed to the actuated cross-piece that moves in a vertical direction. Two types of electrode sets (i.e. S1 and S2, with differing geometry and baking conditions for polyimide) are tested. Once the electrode set is clamped to two aluminum supports at both ends as shown in figure 5, a displacement controlled load is applied at a rate of 1 mm min^{-1} until complete failure of the device is observed. Typical failures are a complete rupture of the electrode set. The parameters recorded are load, deflection, tensile stress (MPa) and tensile strain (%).

3.3. Electrical characterization through impedance spectroscopy

Electrical characterizations consist of ac impedance analysis using a buffer of PBS solution (0.13 M NaCl, 0.022 M $NaH_2PO_4 \cdot H_2O$, 0.081 M $NaH_2PO_4 \cdot 7H_2O$ at pH of ~7.3). The ac impedance measurements are made using Solartron Analytical Model 1070E (AMETEK, Oakridge, TN). This consists of galvanostatic impedance measurement in the frequency range from 1 MHz to 1 Hz (frequency sweep) and amplitude of 10 μA. Several channels of electrode set S1 are tested, along with an on-board reference electrode made of platinum.

4. Results and discussions

A number of useful insights to the chemical, mechanical, and electrical characteristics of glassy carbon electrodes supported on polyimide are obtained through the suite of characterization experiments reported above.

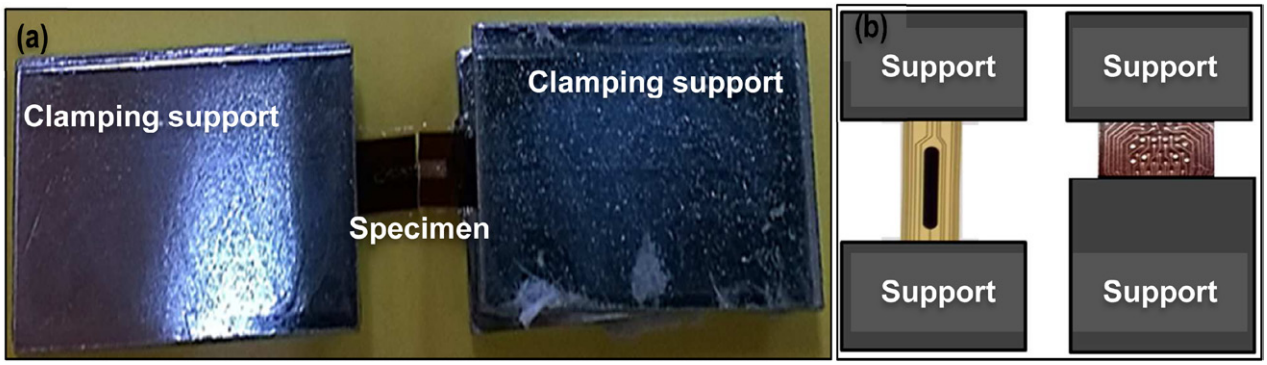

Figure 5. (a) Steel bracket sample holder with electrode set in preparation for tensile test, (b) location of clamp support for both geometries of probes tested. For S1, the area of interest is the upper middle part of the probe with traces and polyimide, whereas for S2, the area of interest consists of electrodes, traces and polyimide substrate.

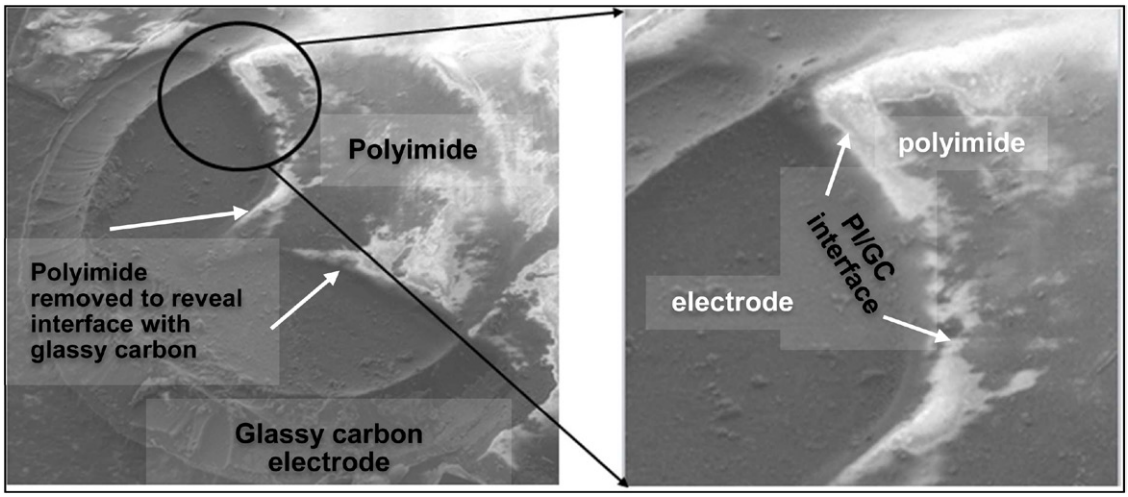

Figure 6. Interface between polymer substrate and glassy carbon electrodes in S1 electrode set. Inset shows a close-up view of polyimide and glassy carbon electrode interface.

4.1. Interfacial chemical bond

Regarding the bond at the interface between the two materials, visual inspection of SEM images as shown in figure 6 demonstrate that the polyimide and glassy carbon electrodes form a homogeneous bond with no noticeable gaps. Further, the figure shows polyimide coating partially removed revealing a surface that seems to stick very well to the glassy carbon surface.

Figures 7(b) and (c) are the overlapped spectra of the polyimide, carbon, and composite structures. These graphs have been baseline corrected and zoomed into the carbonyl area (1600–1800 cm^{-1}) and the carbonyl hydrogen bonding (2550–2650 cm^{-1}) [23, 24]. The durimide has three distinct peaks in the carbonyl region, 1604, 1713, and 1777 cm^{-1}, while the carbon only has one very broad peak at 1637 cm^{-1}. Despite the similarities in the interface and polyimide spectra, a decrease in intensity in all the carbonyl peaks can be seen. This decrease implies a decrease of the three types of carbonyls in the spectra. Since our previous publication showed that the carbon surface carbonyls are due to defects that generate carboxylic acid [25], we propose that the interface under investigation would not be nearly as orderly as the polyimide chains. This will cause not only a decrease in peak intensity but also a broadening of peaks which can be seen as a symmetric broadening at 1777 cm^{-1} and an asymmetric broadening at 1605 cm^{-1}. These changes in the spectra clearly indicate carbon's influence on the bending and vibrational modes of the polyimide carbonyl. In figure 7(c) we see further confirmation of the carbonyl interaction with the carbon by changes in carboxyl dimer peaks at 2660 and 2585 cm^{-1}. While these peaks are present in the durimide, a distinct increase in the broadness at both peaks indicates more unorganized interaction at the interface than between the polymer chains. Taken together, this suggests that (i) the polyimide does not just form carbonyl dimers but carboxylic acid dimers with itself, and (ii) the polyimide forms these same types of dimers via hydrogen bonding with the carbon, not just electrostatic interaction between the carbonyls.

4.2. Modulus and tensile strength

With regard to the mechanical properties of glassy carbon structures supported on polyimide, the modulus is measured for both the electrodes as well as the substrate of probe S3 across multiple cross-sections to give a complete picture of the net modulus of the whole electrode system. As shown in figure 8, the average modulus of glassy carbon

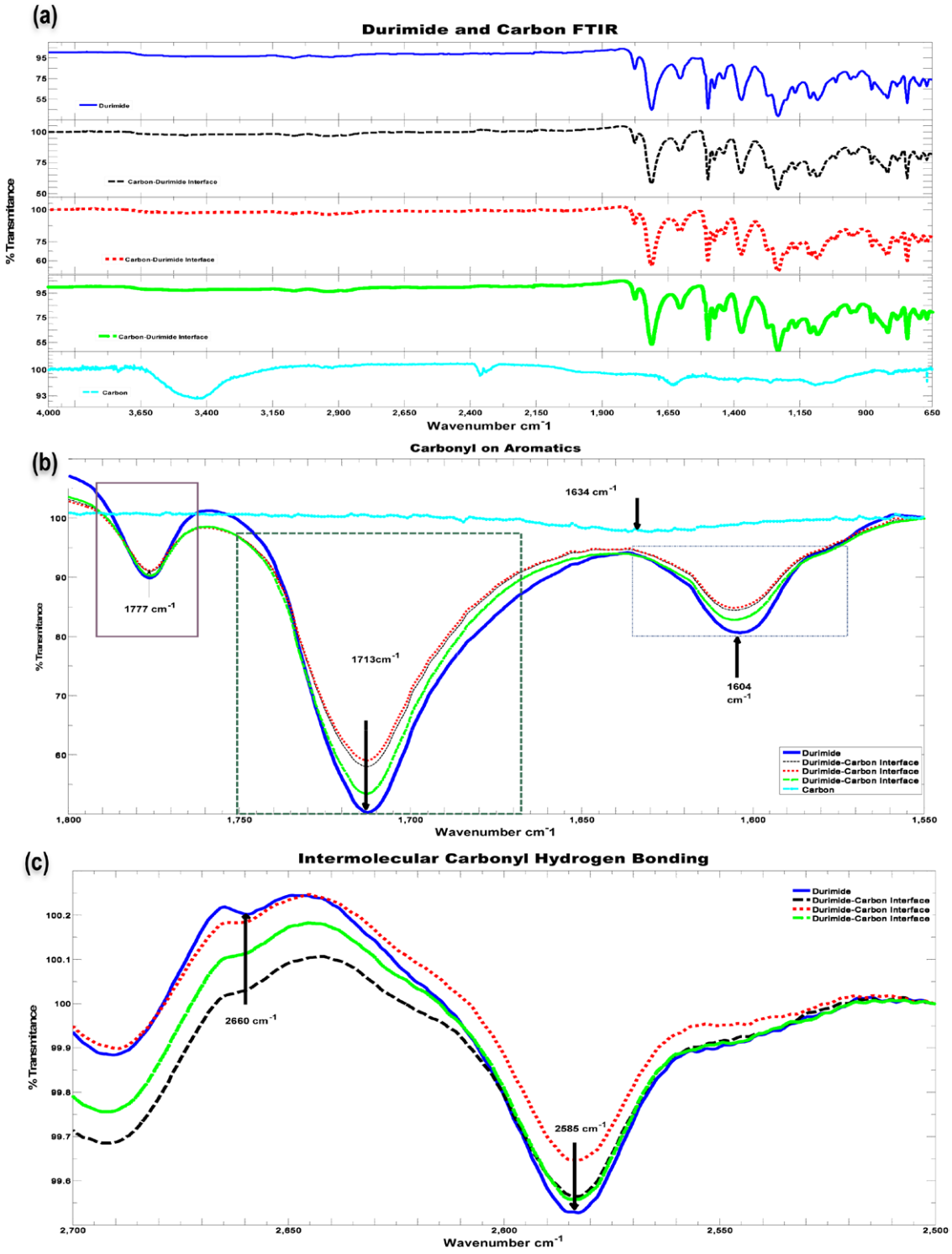

Figure 7. (a) FTIR spectra of polyimide, glassy carbon, and polyimide with glassy carbon showing broadening of carbonyl peaks (b) and carboxylic acid hydrogen bonding peaks (c).

electrodes is measured to be 20 GPa while that of the polyimide substrate was 2.5 GPa. These values correspond very well with what is reported in the literature for glassy carbon [25] and polyimide [26]. Further details are given in previous works [8, 9].

The load–deflection and stress–strain diagrams for both probes S1 and S2 are given in figures 9 and 10. Since probes S1 and S2 are prepared under different conditions, the load–deflection curves and stress–strain diagrams are expected to be different. S1 is processed under a lower temperature of annealing (275 °C) with the intent of avoiding one of the main practical difficulties of polyimide which is a sharp edge at the side ends that has been observed to cause cuts on tissues during implanting. S2, however, is annealed at a vendor-specified much higher temperature of 375 °C resulting in darker and more brittle probes.

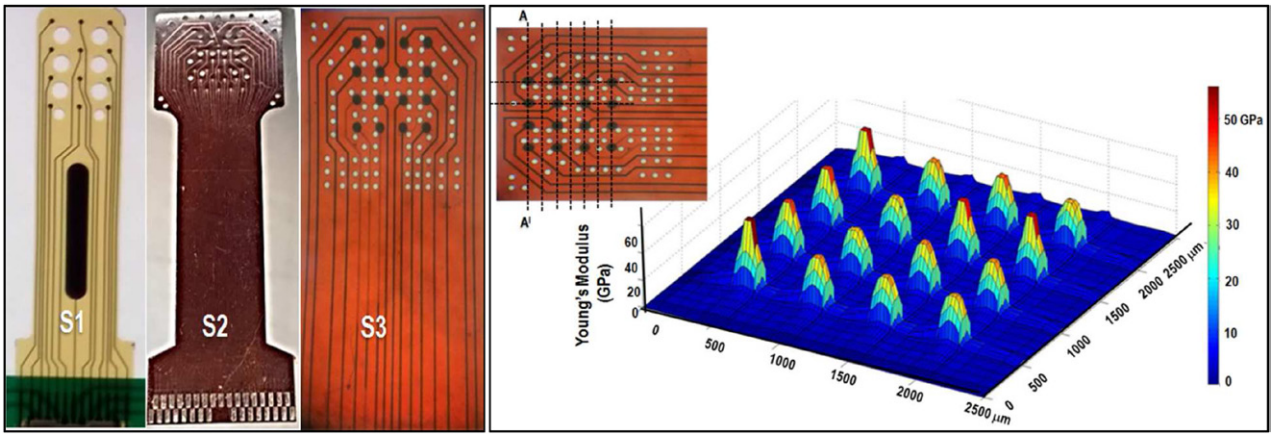

Figure 8. (a) Details of the three neural probes tested here. (b) Mapping of modulus of hybrid glassy carbon and polyimide microstructure (S3) with 4×4 array of microelectrodes using a nanoindenter. Measurements were made at ten points along a typical cross-section (e.g. A–A′) covering both electrodes and polyimide substrate.

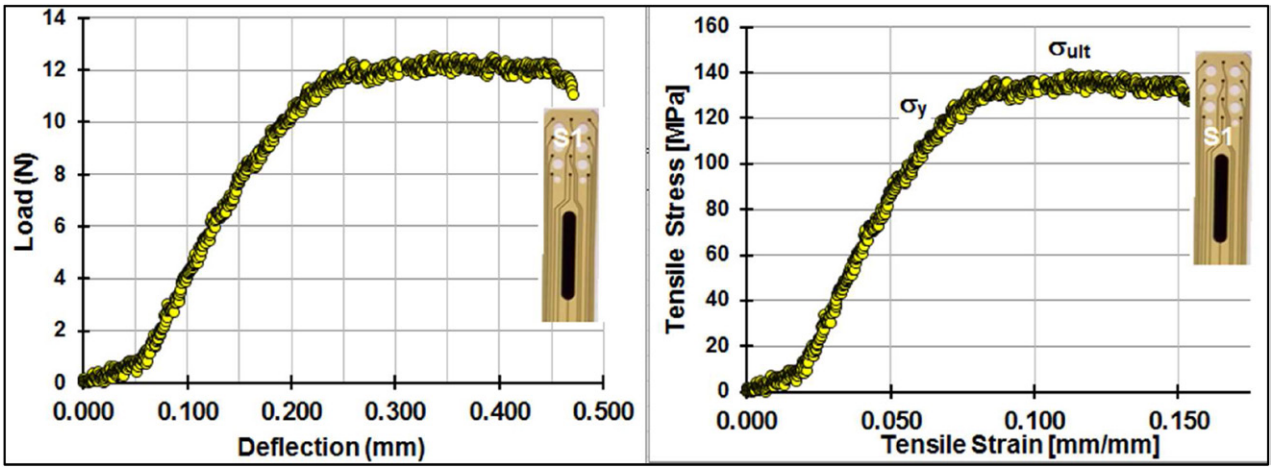

Figure 9. (a) Load–deflection curve and (b) stress–strain curve for the test electrode set sample S1. The yield stress (σ_y) is ~18 MPa while ultimate stress (σ_{ult}) is ~20.9 MPa. The ultimate strain $> 15\%$.

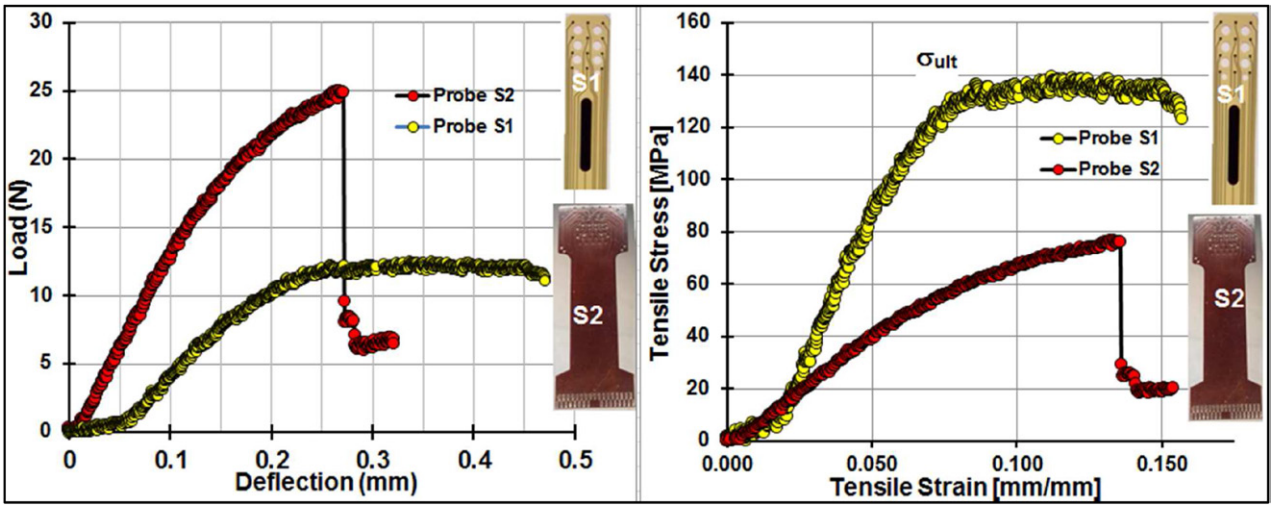

Figure 10. (a) Load–deflection curve and (b) stress–strain curve for two electrode sets fabricated under different conditions demonstrating the influence of fabrication on load carrying capacity and modulus.

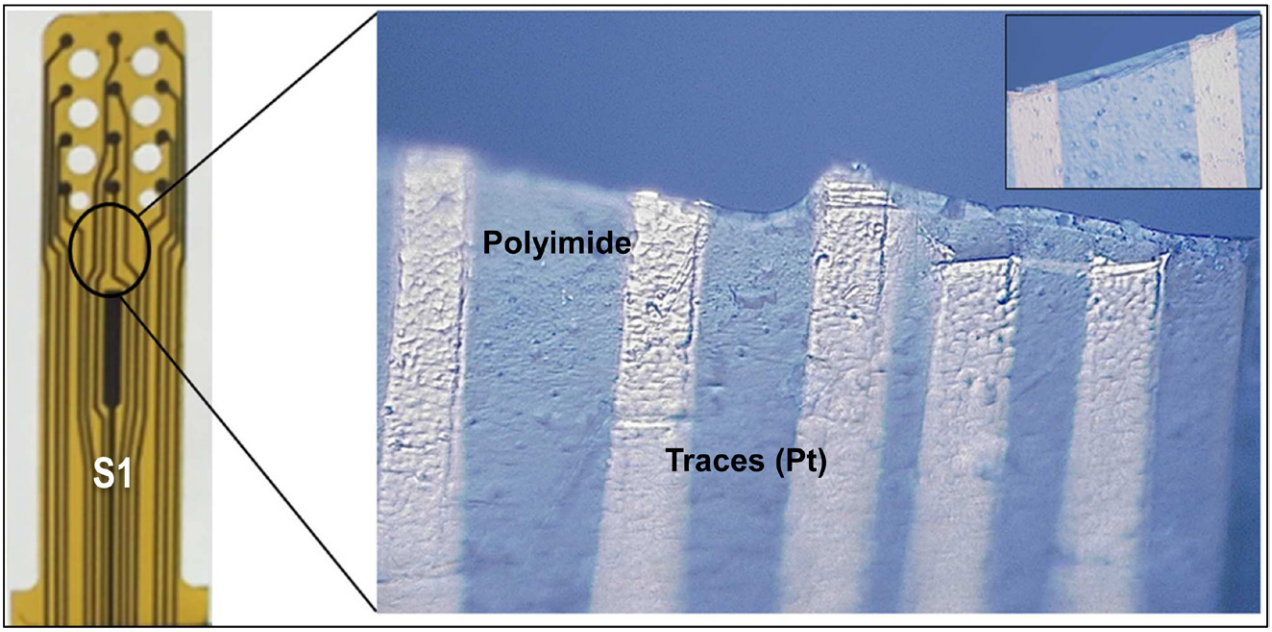

Figure 11. Electrode set S1 after failure during tensile test. The figure shows that the traces and polyimide layer held together as a unit indicating a strong bond between the two. The inset demonstrates that the traces are completely embedded in the polyimide layer and that failure happened along a common plane.

The S1 electrode sets behave elastically up to a strain level of 0.067 mm mm^{-1}. Beyond that, the probe yields and begins displaying plastic behavior before completely failing at a strain of 0.157 mm mm^{-1} (deflection = 0.47 mm). Several electrode sets of type S1 are successfully tested and averages of maximum tensile loading of 12.2 N and modulus of 1.5 GPa are recorded. The S2 electrode set, on the other hand, shows a brittle response with load higher than S1 (25 N), less stress (due to large area), and a maximum deflection of 0.27 mm which is half of the deflection of S1. S2 fails at a lower strain (0.136 mm mm^{-1}) as well. The first failure in S2 is snapping at 0.27 mm deflection due to tearing of breathing holes. The modulus of these probes represents the combined value for glassy carbon traces and polyimide composite material that can be likened, for all practical purposes, to a fiber reinforced material. In general, therefore, the nanoindentation modulus results (2.5 GPA) for probe S3 which was annealed at a higher temperature are observed to be higher than the long-axis modulus of probe S1 which has an average value of 1.5 GPA, but was annealed at a lower temperature. The majority of the variation could be attributed to the effect of annealing with regard to not only the overall mechanical strength of the final polyimide, but also, possibly, anisotropy due to non-uniform annealing in the various directions.

With regard to modes of failures under tensile load, the optical microscopy images of the failed specimen indicating the rupture zones are shown in figures 11(S1) and 12(S2). The images indicate that the glassy carbon electrodes, traces, and polyimide substrate continue to behave as an ideal composite unit until failure where fracture planes actually pass through all these components. The inset in figure 12 shows that the failure plane not only passes through the electrode, but also makes a clean cut underlining the fact that the polyimide and glassy carbon electrode act as one unit. It has to be emphasized that it is indeed remarkable that the electrodes are not pulled out of the substrate, but remain affixed to it until tensile failure occurs. This is an important finding that demonstrates almost a perfect bond between polyimide and glassy carbon electrodes. This, is turn, provides further evidence for the strong hydrogen bond between glassy carbon and polyimide as discussed in section 4.1.

The initiation of failure mechanisms in the probes S1 and S2 also give substantial information regarding the strength of the bond between polyimide, traces and electrodes. In the S1 probe, the failure is initiated along a plane that contains both traces and polyimide substrate suggesting that failure occurred as the tensile strength of the composite was exceeded. In the S2 probe, however, the location of the test sample subjected to tensile test consists of not only electrodes, traces, and substrates, but also breathing holes. The failure in this probe is initiated at area of weakness which is the breathing holes. Once these failed by tearing, the load capacity decreases and the composite structure is strained in a plastic deformation until a rupture plane that passes through traces, electrodes, and polyimide is formed.

4.3. Electrical impedance spectroscopy

With regard to the electrical characterizations, as shown in figure 13, the impedance at 100 Hz (the usual standard frequency for bio-specific applications) for glassy carbon electrodes is between 100–250 KΩ, ideal for surface micro-electrocorticography (μECoG) measurements. The impedance of the platinum reference electrode at ~8 KΩ is much lower than that of the electrodes because of its large area, which is almost 20 times that of the glassy carbon electrodes. To ensure the robustness and stability of the reference electrode (and consequently of the recorded signal), the trace that connects the reference electrode to the printed circuit board (PCB) is shorter and wider than the

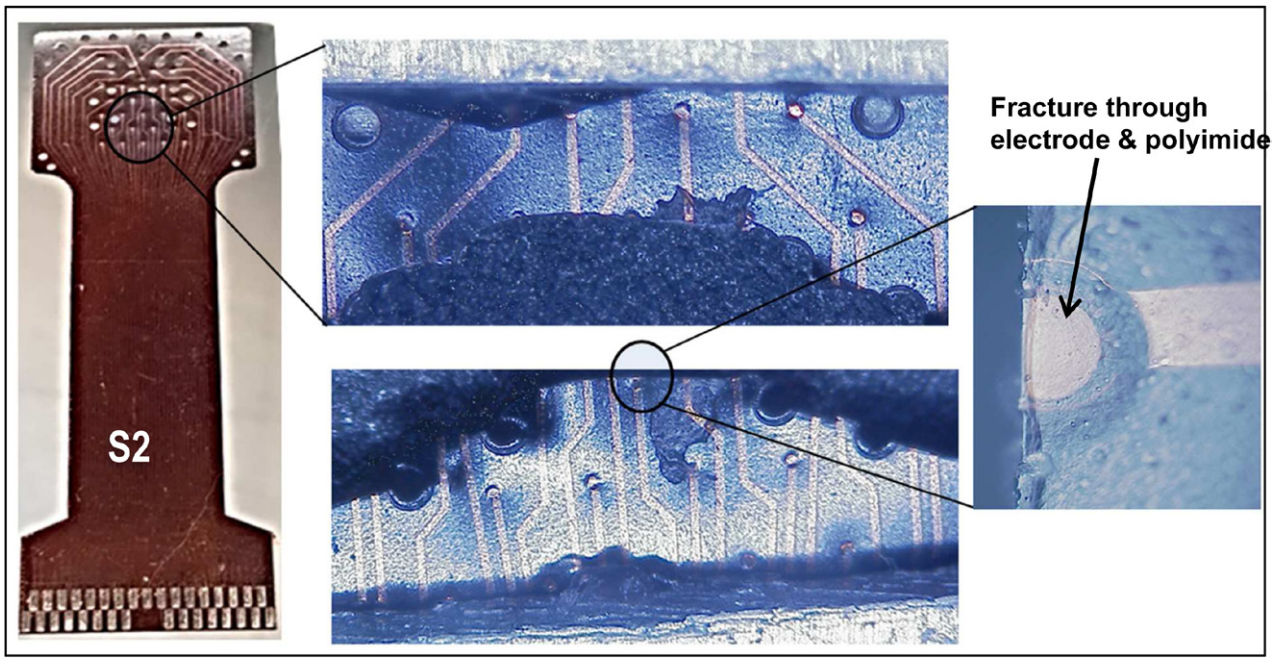

Figure 12. Electrode set S2 after failure during tensile test. Note the failure of the electrode/polyimide interface in the inset demonstrating the rather strong bond between glassy carbon and polyimide. The fracture plane passes through not only the polyimide layer, but also through the electrode and splits it into two pieces. This is an important finding that supports a good mechanical performance on this hybrid structure.

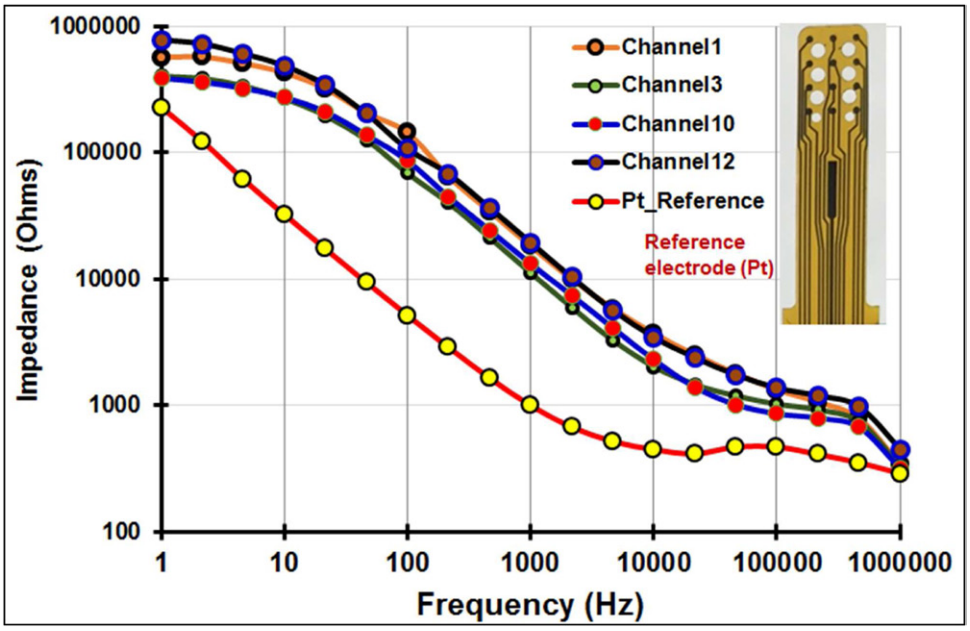

Figure 13. Impedance diagram for different channels of electrode set. The S1 electrode sets have electrodes of 300 μm diameter, and 90 μm wide traces.

traces connecting the glassy carbon electrodes to the same PCB. As a result, we expect the impedance reading of the reference electrode to be stable. On the other hand, as all the electrodes are identical geometrically and process-wise, the impedances are expected to be very close. However, the small difference in impedance readings between each of the channels (electrodes) is possibly caused by differences in impedance of connecting wires as well as the difference in thickness of metal layer of the traces during the metal lift-off process.

5. Conclusions

In this study, we have demonstrated for the first time, not only a novel pattern transferring technique for C-MEMS structures, but also the mechanical, electrical, and chemical characterization of a microelectrode structure consisting of glassy carbon microelectrodes mounted on a flexible and stretchable polyimide substrate. Our findings in this study supported by FTIR spectroscopy indicate a strong hydrogen bonding between

polyimide and glassy carbon expressed as carbonyl peaks due to hydrogen bonding of carbon hydroxyls with the carbonyls on the polyimide. Further, FTIR spectroscopy of polyimide and glassy carbon interface spectra also established a symmetric broadening at 1777 cm^{-1} and asymmetric broadening at 1605 cm^{-1} which indicate carbon's influence on the bending and vibrational modes of the polyimide carbonyl. Additional confirmation of carbonyl interaction with the carbon is shown through a distinct increase in the broadness in carboxyl dimer peaks at 2660 and 2585 cm^{-1} which indicates more unorganized interaction at the interface than between the polymer chains. FTIR spectroscopy also clearly shows that polyimide forms carboxylic acid dimers via hydrogen bonding with the carbon. Mechanical tensile testing results support the presence of a strong hydrogen bond at the polyimide/glassy carbon interface resulting in failure planes that pass through not only the polyimide, but through both polyimide and electrodes.

In general, as shown here, the unique architecture presented combines the unique electrical and electrochemical properties of glassy carbon with metals and, with its flexible substrate mounting, offers a new platform for electrical sensing and actuating probes. Further, such a pattern transfer technology that makes C-MEMS technology useful to a wider user base will enable the field of C-MEMS to move forward in new and exciting directions.

Acknowledgments

This material is based on research work supported by National Science Foundation Grant Number EEC-1028725 under the ERC program. The authors would also like to thank Dr Moon of SDSU for the use of nano-indentation system, Dr Barlow for the use of SEM facilities, and Dr David Pullman for FTIR support.

References

[1] Wang Y, Pham L, de Vasconcellos G P S and Madou M J 2010 Fabrication and characterization of micro PEM fuel cells using pyrolyzed carbon current collector plates *J. Power Sources* **195** 4796–803

[2] Lin P, Park B and Madou M 2008 Development and characterization of a miniature PEM fuel cell stack with carbon bipolar plates *J. Power Sources* **176** 207–14

[3] Kassegne S *et al* 2012 Organic MEMS/NEMS-based high-efficiency 3D ITO-less flexible photovoltaic cells *J. Micromech. Microeng.* **22** 115015

[4] Martinez-Duarte R, Renaud P and Madou M J 2011 A novel approach to dielectrophoresis using carbon electrodes *Electrophoresis* **32** 2385–92

[5] Martinez-Duarte R, Gorkin Iii R A, Abi-Samra K and Madou M J 2010 The integration of 3D carbon-electrode dielectrophoresis on a CD-like centrifugal microfluidic platform *Lab Chip* **10** 1030–43

[6] Hirabayashi M, Mehta B, Nguyen B and Kassegne S 2014 DNA Immobilization on high aspect ratio glassy carbon (GC-MEMS) microelectrodes for bionanoelectronics applications *J. Microsyst. Technol.* **21** 2359–65

[7] Vahidi N, Hirabayashi M, Mehta B, Khosla A and Kassegne S 2014 Bionanoelectronics platform with DNA molecular wires attached to high aspect-ratio 3D metal microelectrodes *ECS J. Solid State Sci. Technol.* **3** Q29–36

[8] Kassegne S *et al* 2015 Electrical impedance, electrochemistry, mechanical stiffness, and hardness tunability in glassy carbon MEMS μECoG electrodes *J. Microelectron. Eng.* **133** 36–44

[9] Kassegne S K, Vomero M, van Niekerk P and Hirabayashi M 2015 Glassy carbon microelectrodes for neural signal sensing and stimulation *C-MEMS Handbook* (New York: Momentum Press)

[10] Ranganathan S, McCreey R, Majji S M and Madou M 2000 Photoresist-derived carbon for microelectromechanical systems and electrochemical applications *J. Electrochem. Soc.* **147** 277–82

[11] Wang C, Taherabadi L, Jia G and Madou M 2005 A novel method for the fabrication of high-aspect ratio C-MEMS structures *J. Microelectromech. Syst.* **14** 348

[12] Rubehn B and Stieglitz T 2010 *In vitro* evaluation of the long-term stability of polyimide as a material for neural implants *Biomaterials* **31** 3449–58

[13] Georgiev A, Dimov D, Spassova E, Assa J, Danev G and Dineff P 2012 Chemical and physical properties of polyimides: biomedical and engineering applications *High Performance Polymers—Polyimides Based—From Chemistry to Applications* (Rijeka: InTech) p 41500

[14] Kato Y X, Furukawa S, Samejima K, Hironaka N and Kashino M 2012 Photosensitive-polyimide based method for fabricating various neural electrode architectures *Front. Neuroeng.* **5** 11

[15] Chen Y Y, Lai H Y, Lin S H, Cho C W, Chao W H, Liao C H, Tsang S, Chen Y F and Lin S Y 2009 Design and fabrication of a polyimide-based microelectrode array: application in neural recording and repeatable electrolytic lesion in rat brain *J. Neurosci. Methods* **182** 6–16

[16] Seoa J M, Kimb S J, Chunga H, Kimb E T, Yua H G and Yua Y S 2004 Biocompatibility of polyimide microelectrode array for retinal stimulation *Mater. Sci. Eng.* C **24** 185–9

[17] Humayun M S, de Juan E Jr, Weiland J D, Dagnelie G, Katona S, Greenberg R and Suzuki S 1999 Pattern electrical stimulation of the human retina *Vis. Res.* **39** 2569–76

[18] Young J T *et al* 1993 Non-destructive characterization of polymide/copper and polyimide/gold interphases using surface-enhanced Raman scattering and reflection-absorption infrared spectroscopy *Surf. Interface Anal.* **20** 341–51

[19] Young J T *et al* 1994 Surface-enhanced Raman scattering as an *in situ* probe of polyimide/silver interphases *J. Adhes.* **46** 243–64

[20] Hwa Jin K *et al* 2009 Surface modification of polyimide film by coupling reaction for copper metallization *J. Ind. Eng. Chem.* **15** 23–30

[21] Lee W-J *et al* 2003 Adhesion and interface chemical reactions of Cu/Polyimide and Cu/TiN by XPS *Appl. Surf. Sci.* **205** 128–36

[22] Siow K S, Britcher L, Kumar S and Griesser H J 2006 Plasma methods for the generation of chemically reactive surfaces for biomolecule immobilization and cell colonization-a review *Plasma Process. Polym.* **3** 392–418

[23] Bellamy L J 1975 Amides, Proteins, and Polypeptides *The Infra-Red Spectra of Complex Molecules* (Berlin: Springer) pp 231–62

[24] Hirabayashi M, Mehta B, Vahidi N, Khosla A and Kassegne S 2013 Functionalization and characterization of pyrolyzed polymer based carbon microstructures for bionanoelectronics platform *J. Micromech. Microeng.* **23** 115001

[25] Schueller O J A, Brittain S T, Marzolin C and Whitesides G M 1997 Fabrication and characterization of glassy carbon MEMS *Chem. Mater.* **9** 1399–406

[26] Allen M G, Mehregany M, Howe R T and Senturia S D 1987 Microfabricated structures for the *in situ* measurement of residual stress, Young's modulus and ultimate strain of thin film *Appl. Phys. Lett.* **51** 241–3